ANALYSIS OF STEADY-STATE VEHICLE HANDLING AND DRIVER BEHAVIOUR AT EXTREME DRIVING CONDITIONS

Johannes Edelmann[1], Manfred Plöchl[1] and Peter Pfeffer[2]
[1]Institute of Mechanics and Mechatronics,
Vienna University of Technology,
Wiedner Hauptstraße 8-10, 1040 Vienna, Austria
manfred.ploechl@tuwien.ac.at
[2]Munich University of Applied Sciences,
Faculty 03, Dachauer Straße 98b,
80335 Munich, Germany

Abstract

At steady-state cornering multiple handwheel steering angles are possible to accomplish the same cornering radius at the same speed. Although some of the corresponding driving states may be considered extreme, at least the powerslide motion can be observed in rallye sports. The powerslide involves a large side slip angle of the vehicle, large traction forces and countersteering, and generally needs to be stabilized by the driver. A respective human-like driver model, capable of handling large side slip angles of the vehicle and the essential influence of traction forces on lateral tyre forces, is introduced and provides the required steering and longitudinal control to hold the vehicle on a circular, low friction track. Besides measurements from test runs, numerical results are presented to reveal some basic influences of the tyre characteristics on the handling diagram at extreme driving conditions.

1 INTRODUCTION

Vehicle models for numeric simulation of the dynamics of automobiles have become increasingly complex in recent years. The aim to simulate real dynamic behaviour brought engineers to include a high level of detail in their vehicle models, facilitated by the application of multibody dynamics software. Basic vehicle models are popular in control design, however they are still indispensable to reveal and understand basic dynamic phenomena.

Handling characteristics of automobiles have been investigated over many decades, leading to a deep insight into the steering and stability properties of automobiles, [1, 2] as an example of early contributions. Considering extreme driving conditions however, there are still phenomena, well-known from observations, which deserve closer attention.

Inspired from observations in rallye sports, measurements of large side slip manoeuvres have been presented in [3]. On the basis of a simple nonlinear four-wheel vehicle model with rear-wheel drive and a tyre model, that comprises the mutual influence of longitudinal and lateral tyre forces, up to four different steering angles have been numerically identified for steady-state cornering at the same speed and cornering radius, [4]. These results have been supported by measurements. Stability analysis in [5] reveals the unstable nature of two of these steady-state solutions including the powerslide motion. Powerslide of an automobile is defined in [5] as a steady-state cornering motion with a large side slip angle of the vehicle, considerably large traction forces and a steering angle towards the outside of the curve (countersteering). Performing an autonomous powerslide has been studied and experimentally tested in [6, 7]. The powerslide motion is stabilized in [7] by an automatic steering controller, in [8] by controlling driving/braking torques of the front and rear wheels at a constant steering angle, and in [9] by a sliding mode control using steering angle and driving torque inputs.

Skilled rallye drivers may prefer to perform a powerslide, when negotiating a curve, in particular on gravel roads (low friction surfaces). One can think of several reasons therefore: saving time in the curve, less sensitive and thus easier to control for the driver with respect to unexpected disturbances (e.g. varying track conditions) in contrast to regular driving, vehicle is early aligned to the following road segment, and last but not least, maximum exit velocity. Path optimization including the powerslide is discussed in [10]. The authors conclude, when a straight follows a corner, the driver is able to fully accelerate while still in the corner, thus maximizing the velocity at the exit of the corner. Except for the driver steering model in [11], driver models do in general not cover the powerslide motion. In this case, the driver model must in particular be able to deal with large side slip angles of the vehicle and the influence of traction forces on the lateral tyre forces.

In this paper tyre characteristics are investigated in more detail by applying a nonlinear vehicle model to better understand their effect on the appearance of different extreme driving states, like the powerslide, at steady-state cornering. As the powerslide needs to be generally stabilized by the driver to take an advantage from performing a powerslide, attention is given to the respective demands on the driver and a corresponding driver model is introduced.

In Section 2 the applied vehicle model is addressed, in Section 3 measurements for validation are shown. The influence of the tyre characteristics on the analytically derived handling curves is discussed briefly in Section 4, and a driver model, which is able to stabilize also a powerslide motion and to track a given trajectory, is presented in Section 5.

2 VEHICLE MODEL

For analytical investigation, the equations of motion of a basic nonlinear four-wheel vehicle model of an automobile with rear-wheel drive, Fig. 1(a), are specified in this section. With velocity v, side slip angle β of the vehicle, yaw

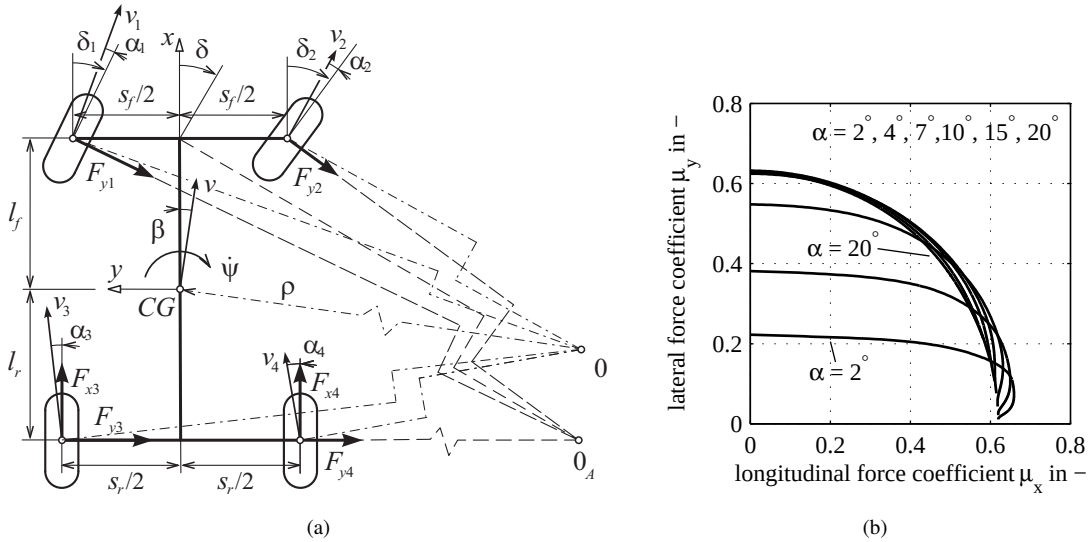

(a) (b)

Figure 1 (a) Four-wheel vehicle model with rear-wheel drive at regular cornering
(b) Nonlinear steady-state tyre characteristics (rear tyre, wet surface)

rate $\dot{\psi}$ and front wheel steering angles δ_1 and δ_2, the relations

$$\tan(\delta_1-\alpha_1)=\frac{l_f\dot{\psi}+v\sin\beta}{v\cos\beta+\dot{\psi}s_f/2},\quad \tan(\delta_2-\alpha_2)=\frac{l_f\dot{\psi}+v\sin\beta}{v\cos\beta-\dot{\psi}s_f/2},$$
$$\tan\alpha_3=\frac{l_r\dot{\psi}-v\sin\beta}{v\cos\beta+\dot{\psi}s_r/2},\quad \tan\alpha_4=\frac{l_r\dot{\psi}-v\sin\beta}{v\cos\beta-\dot{\psi}s_r/2}, \tag{1}$$

to calculate the tyre side slip angles α_i (i = 1-4) can be read off Fig. 1(a), as well as the geometric relations

$$\frac{(l_f+l_r)}{\tan\delta_1}=\frac{(l_f+l_r)}{\tan\delta}+\frac{s_f}{2},\quad \frac{(l_f+l_r)}{\tan\delta_2}=\frac{(l_f+l_r)}{\tan\delta}-\frac{s_f}{2}, \tag{2}$$

to realize Ackermann steering behaviour. The steering angle δ is considered as one of two input variables to the vehicle controlled by the driver. The other input variable, the driving torque M, is distributed equally to both rear wheels by an open differential gear at the considered rear-wheel drive. Therewith Euler's law gives

$$I_\omega\dot{\omega}_3=M/2-F_{x3}r\quad\text{and}\quad I_\omega\dot{\omega}_4=M/2-F_{x4}r, \tag{3}$$

with loaded radius r and the moment of inertia I_ω of a single wheel. The angular velocities ω_3 and ω_4 of the rear wheels relate the longitudinal velocities of the corresponding wheel centres to the longitudinal slip values s_{x3}, s_{x4}, which are required to calculate the respective longitudinal tyre forces F_{x3}, F_{x4}. Again geometric and kinematic considerations yield (rolling radius $\bar{r}\approx r$)

$$s_{x3}=-\frac{(v\cos\beta+\dot{\psi}s_r/2)-\bar{r}\omega_3}{v\cos\beta+\dot{\psi}s_r/2},\quad s_{x4}=-\frac{(v\cos\beta-\dot{\psi}s_r/2)-\bar{r}\omega_4}{v\cos\beta-\dot{\psi}s_r/2}. \tag{4}$$

The equations of motion of the vehicle model are derived by neglecting chassis roll, pitch and heave dynamics. Aerodynamic properties of the vehicle, tyre rolling resistance and the influence of the inertia of the wheels on the global vehicle motion are disregarded. Also the suspension systems are not modelled in detail. With these

simplifications, the equations of motion are found from Newton's and Euler's law:

$$\begin{aligned}
m\dot{v}\cos\beta - mv(\dot{\beta}+\dot{\psi})\sin\beta &= F_{x3}+F_{x4}-F_{y1}\sin\delta_1-F_{y2}\sin\delta_2\,,\\
m\dot{v}\sin\beta + mv(\dot{\beta}+\dot{\psi})\cos\beta &= F_{y1}\cos\delta_1+F_{y2}\cos\delta_2+F_{y3}+F_{y4}\,,\\
0 &= F_{z1}+F_{z2}+F_{z3}+F_{z4}-mg\,,\\
0 &= (F_{z1}-F_{z2})s_f/2+(F_{z3}-F_{z4})s_r/2-(F_{y1}\cos\delta_1+F_{y2}\cos\delta_2+F_{y3}+F_{y4})h\,,\\
0 &= -(F_{z1}+F_{z2})l_f+(F_{z3}+F_{z4})l_r+(F_{y1}\sin\delta_1+F_{y2}\sin\delta_2-F_{x3}-F_{x4})h\,,\\
I_z\ddot{\psi} &= (-F_{y1}\sin\delta_1+F_{y2}\sin\delta_2)s_f/2+(F_{x3}-F_{x4})s_r/2+(F_{y1}\cos\delta_1+F_{y2}\cos\delta_2)l_f-(F_{y3}+F_{y4})l_r\,.
\end{aligned} \tag{5}$$

The total vehicle mass is denoted m, the yaw moment of inertia I_z, and the height of the centre of gravity (*CG*) above ground h. The degree of freedom of the resulting vehicle model is five: v, ψ, β, ω_3, ω_4.

Assuming small roll and pitch angles and a linear relation between the vertical tyre forces F_{zi} and the corresponding vertical deflections z_i of the suspension springs, the geometric constraint $z_1 s_r + z_4 s_f = z_2 s_r + z_3 s_f$ results in the relationship $(F_{z1}-F_{z2})\,s_r c_r = (F_{z3}-F_{z4})\,s_f c_f$. The roll stiffness of the front and rear torsion bars is included in the front and rear suspension rates c_f and c_r, respectively. Consequently, the suspension systems will map the front/rear and left/right load transfer, only.

Due to the rear-wheel drive, the front lateral tyre forces depend only on the corresponding side slip angles and wheel loads, $F_{y1} = F_{y1}(\alpha_1, F_{z1})$, $F_{y2} = F_{y2}(\alpha_2, F_{z2})$, whereas the rear lateral tyre forces additionally depend on the corresponding longitudinal tyre slips, $F_{y3} = F_{y3}(\alpha_3, s_{x3}, F_{z3})$, $F_{y4} = F_{y4}(\alpha_4, s_{x4}, F_{z4})$, due to possibly large rear traction forces $F_{x3} = F_{x3}(\alpha_3, s_{x3}, F_{z3})$, $F_{x4} = F_{x4}(\alpha_4, s_{x4}, F_{z4})$. The applied steady-state tyre characteristics, for details see [12], are shown in Fig. 1(b) with an estimated maximum force coefficient $\mu_{\max} = 0.67$ (for a given nominal vertical tyre force $F_{z,\mathrm{nom}} = 5800$ N) and a sliding coefficient of friction $\mu_g = 0.62$, representing tyre – wet asphalt contact conditions. The transient tyre behaviour is modelled by a first order time lag using longitudinal and lateral relaxation lengths.

3 MODEL VALIDATION AT STEADY-STATE CORNERING

Steady-state solutions (marked with subscript 0) are numerically calculated by solving the equations of motion in Eq. (5) with steady-state conditions $\dot{v} = 0$, $\ddot{\psi} = 0$, $\dot{\beta} = 0$, $\dot{\omega}_3 = 0$, $\dot{\omega}_4 = 0$ and $\dot{\psi} = v_0/\rho$ for a given constant radius ρ at different velocities v_0. In the handling diagrams of Fig. 2 the steering angle δ and the side slip angle β of the vehicle are plotted against the normal acceleration v^2/ρ for an SUV on a wet circular track with $\rho = 50$ m in Fig. 2(a), and for a sports car on an icy circular track with $\rho = 100$ m, Fig. 2(b). Fig. 2(a) reveals, that, besides the regular cornering solution, characterized by small steering and side slip angles, up to three additional steady states at cornering for a given velocity v are possible, resulting in two branches with (large) positive steering angles (both dashed) – called here overdraw steering – and the powerslide branch with large negative steering angles.

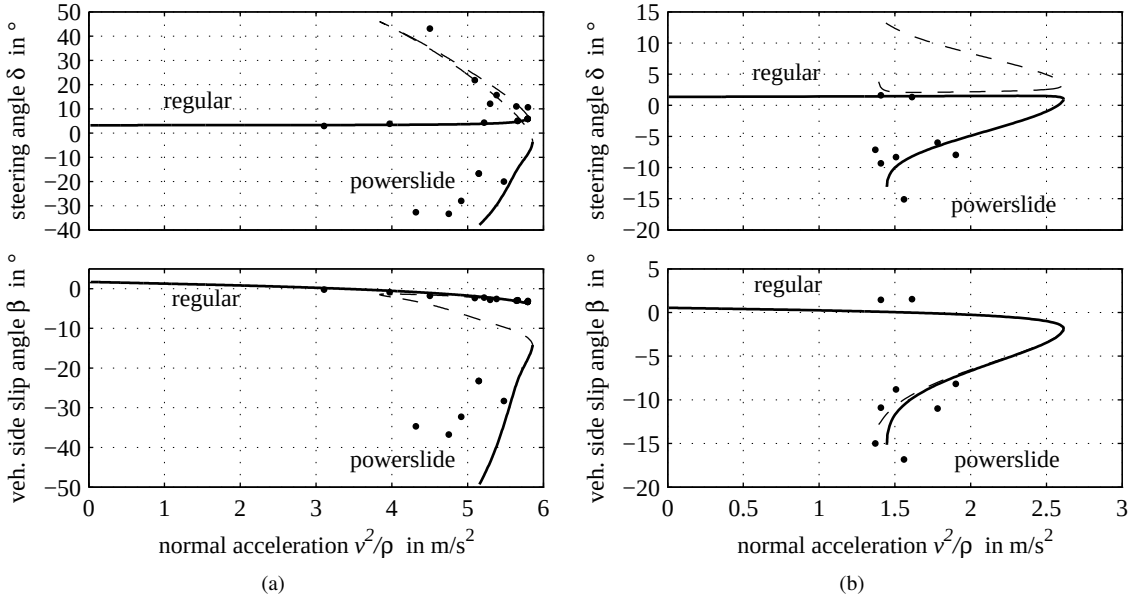

Figure 2 Steady-state handling characteristics on (a) wet surface with an SUV, $\rho = 50$ m, [5], and on (b) icy surface with a sports car, $\rho = 100$ m; measured data points (•) and numerical results (–)

Besides main parameters of both vehicles, e.g. [5], measurements of a winter tyre on a drum test stand were available for the tyre characteristics on icy surface. As the surface temperature of −4 ° of the artificial ice was considerably higher than the temperature of the ice at the test runs, the parameters for the tyre model [12] had to

be scaled by a factor of 1.4 to meet the measured maximum force coefficient. Missing tyre parameters had to be estimated. Although there are deviations due to the mentioned model simplifications and uncertainties related to the tyre model parameters, the overall characteristics of the calculated results match quite well to the measurements.

4 BASIC ANALYSIS OF EXTREME HANDLING CHARACTERISTICS

Numeric results and their discussion in this section are based on the sports car, with main vehicle parameters $m = 1600$ kg, $l_f = 1.41$ m, $l_r = 0.94$ m, $s_f = 1.485$ m, $s_r = 1.520$ m, see Fig. 1(a), performing steady-state cornering at $\rho = 100$ m on wet surface, Fig. 1(b). For clearness, steady-state solutions impossible or useless from a technical point of view, have not been omitted.

When neglecting the wheel load transfer front/rear, left/right, by applying a nonlinear two-wheel instead of a four-wheel vehicle model, the characteristics of the handling diagram in Fig. 3(a) may change considerably. For example, points O_1, O_2 have no equivalent in the handling curve of the two-wheel vehicle model. Nevertheless, the area of practically reasonable powerslide is quite similar. To match measurements with numerical results however, the four-wheel vehicle model is essential. With increasing vehicle side slip angle in the powerslide motion, the wheel load transfer left/right decreases, while loads are shifted to the rear, advantageous to apply large traction forces. Note the qualitatively different handling curve characteristics for wet and icy surface in Fig. 2(b) and that the maximum velocity (normal acceleration) is already in the powerslide branch with $\beta = -13\,^\circ$.

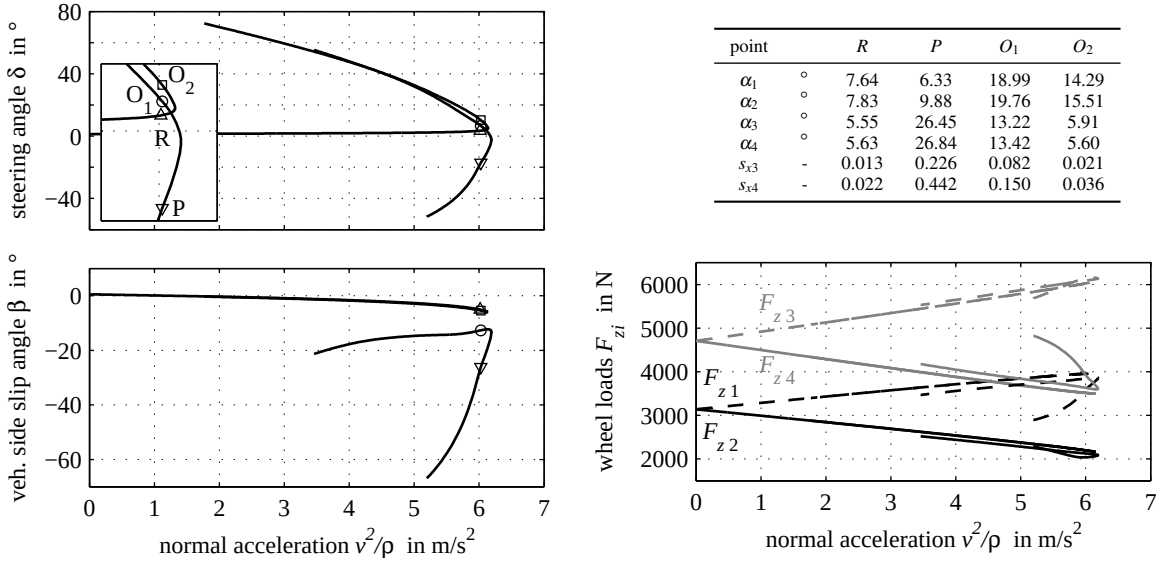

point		R	P	O_1	O_2
α_1	°	7.64	6.33	18.99	14.29
α_2	°	7.83	9.88	19.76	15.51
α_3	°	5.55	26.45	13.22	5.91
α_4	°	5.63	26.84	13.42	5.60
s_{x3}	-	0.013	0.226	0.082	0.021
s_{x4}	-	0.022	0.442	0.150	0.036

Figure 3 (a) Steady-state handling characteristics of the four-wheel vehicle model of the sports car on wet surface and (b) corresponding wheel loads

Generally speaking, the overdraw steering branches are a result of the lateral saturation property of the front tyres. Without saturation no overdraw steering branch appears, and oversteer behaviour shows up for higher normal accelerations. For the front tyres the longitudinal slip (not considered here) is small enough to neglect its influence on the lateral tyre force. The front tyre characteristics are here in particular important for the desired regular over/understeer behaviour.

Fig. 3(a) represents typical (extreme) handling curves with understeer behaviour at lower normal accelerations. While vehicle side slip angles, and side slip angles and longitudinal slips of the rear tyres are relatively small for the overdraw steering branch following the regular branch, e.g. point O_2, the nonlinear lateral tyre characteristics are relevant for the front tyres for both overdraw steering branches, see points O_2 and O_1. For the latter overdraw steering branch and the powerslide branch, point P, all horizontal tyre forces are in general saturated. Additionally, the consideration of the decreasing effect of large longitudinal slips on the rear lateral tyre forces is essential for the onset of both branches. As a consequence, the corresponding mathematical relation in particular, as well as the relation between maximum force coefficient and sliding friction coefficient, are constructive for the design of the handling curves at higher normal accelerations. At the handling characteristics for oversteer behaviour at lower normal accelerations the powerslide branch typically follows the regular branch.

Although handling curves do change, when considering velocity dependent tyre characteristics for wet surface, the principal statements above still hold as simulations have shown. Due to missing corresponding tyre measurements, the velocity influence has been neglected here.

5 DRIVER MODEL TO PERFORM A POWERSLIDE

The driver is capable of drawing on knowledge of the vehicle dynamics of past driving experience to generate vehicle steering commands, [13]. This capability is represented by a set of locally linearized internal vehicle models and designated the "internal model family concept", [13], where the unskilled driver has only knowledge on the range of linear vehicle behaviour, while the expert driver has knowledge on the nonlinear range too. This concept has also been used in [14] to represent driver behaviour at high lateral accelerations and is now extended to the powerslide regime.

As the powerslide motion is inherently unstable, [5], the driver has to stabilize the motion of the vehicle besides compensating deviations from the demanded vehicle trajectory. Measurements show that the driver applies both steering and throttle inputs while performing a quasi steady-state powerslide, see [3, 5, 9]. Controllability analysis of the vehicle at powerslide motion reveals that the motion can be stabilized by steering wheel or throttle inputs only as well as by a applying both of them.

It is assumed that the driver's task is separated into a stabilizing task and a path keeping task: while the motion of the vehicle is stabilized with both steering inputs and torque inputs distributed to the rear wheels, $\Delta\delta_s$ and ΔM_s respectively, or ΔM_s inputs only, path keeping of the stabilized vehicle is realized by additional steering inputs $\Delta\delta_c$, similar to regular driving, see Fig. 4. As the driver has to keep the vehicle on a circle at constant speed, the anticipated (feed forward) steering angle δ_a, [14], is the constant steady-state steering angle δ_0 in this case, and the driving torque distributed to the rear wheels, required to maintain the desired speed, is $M_a = M_0$.

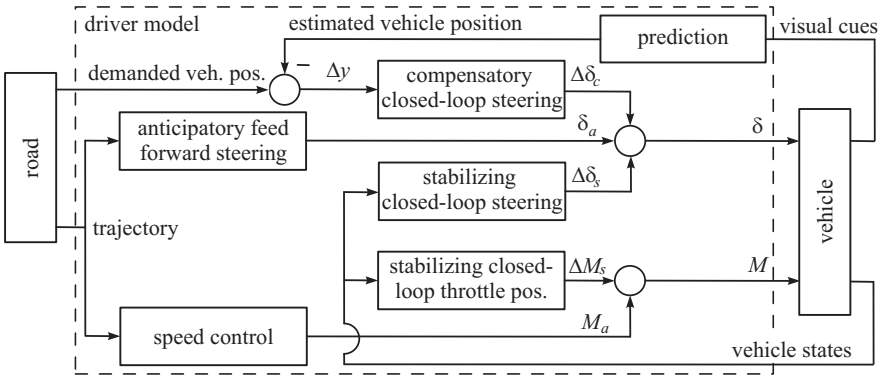

Figure 4 Driver model block diagram

The internal vehicle model of the driver is represented by the nonlinear, two-wheel vehicle model

$$mv\left(\dot{\beta}+\dot{\psi}\right)\cos\beta = F_{yf}\cos\delta + F_{yr}\,, \quad I_z\ddot{\psi} = F_{yf}l_f\cos\delta - F_{yr}l_r\,, \tag{6}$$

where the front and rear substitutive lateral tyre forces F_{yf} and F_{yr} are represented by

$$F_{yf} = F_{yf}\left(\alpha_f\left(\delta,\beta,\dot{\psi}\right)\right), \quad F_{yr} = F_{yr}\left(\alpha_r\left(\beta,\dot{\psi}\right), F_{xr}(M)\right). \tag{7}$$

Applying a local linearization with respect to the vehicle states β and $\dot{\psi}$ and the driver's inputs δ and M at steady-state cornering, the state-space representation

$$\Delta\dot{\underline{x}} = \mathbf{A}\Delta\underline{x} + \mathbf{B}\Delta\underline{u}_s + \underline{b}\Delta\delta_c \tag{8}$$

is derived, where Δ denotes deviations from the trim condition, $\Delta\underline{x} = [\Delta\beta\ \ \Delta\dot{\psi}]^{\mathrm{T}}$, $\Delta\underline{u}_s = [\Delta\delta_s\ \ \Delta M_s]^{\mathrm{T}}$ and $\Delta\delta = \Delta\delta_s + \Delta\delta_c$ if the vehicle is stabilized with both steering and torque inputs, or $\Delta\underline{u}_s = \Delta M_s$ and $\mathbf{B} = \underline{\tilde{b}}$ if it is stabilized with torque inputs only. For simplicity a state feedback control $\Delta\underline{u}_s = -\mathbf{R}\Delta\underline{x}$ is applied for the stabilization task of the driver, where the unstable pole is shifted from the positive to the negative half plane.

To determine the parameters for the compensatory closed-loop control layer, the transfer function $\Delta y_{CG}/\Delta\delta_c$ between the correction steering angle $\Delta\delta_c$ and the distance Δy_{CG} of the CG of the vehicle to the demanded trajectory, is derived from the stablilized system $\Delta\dot{\underline{x}} = (\mathbf{A}-\mathbf{BR})\Delta\underline{x} + \underline{b}\Delta\delta_c$, similar to [14]. With the prediction function $\Delta y/\Delta y_{CG} = 1 + T_p s + \left(T_p^2/2\right)s^2$ (in frequency domain; in time domain the current cornering radius is used to estimate Δy after T_p), where T_p denotes the preview time, the driver finally compensates predicted future path deviations Δy with the correction steering angle δ_c, [15],

$$\frac{\Delta\delta_c}{\Delta y} = V_c\frac{1+T_v s}{1+T_n s}\mathrm{e}^{-T_r s}. \tag{9}$$

T_v, T_n and V_c are driver properties that are derived to achieve given dominant poles of the closed-loop "vehicle-driver", a demanded stability margin and a gain decline of -20 dB/decade of the open-loop system in the vicinity of the crossover frequency (approximately 0.4 Hz) according to [15]. The human reaction time is set to $T_r = 0.1$ s. This time delay has also been applied to the stabilizing closed-loop control layer.

Starting from the powerslide motion indicated with point P ($\triangledown$) in Fig. 3(a), the vehicle suddenly encounters a small, dry surface area. The level of available friction is instantaneously changed for our wheels as kind of

impulse disturbance. From Fig. 5 it becomes obvious, that the motion can be stabilized by the driver model, in the presented case with combined, quite excessive driving torque and steering inputs, and the circular trajectory with radius $\rho = 100$ m is tracked. Driver parameter determination suggests the need of a considerably shorter preview time T_p and larger steering gain V_c compared to parameters required for regular driving, point R ($\triangle$) in Fig. 3(a) ($l_p = v_0 T_p = 7.5$ m and 30 m, $V_c = 0.54$ rad/m and 0.012 rad/m, respectively).

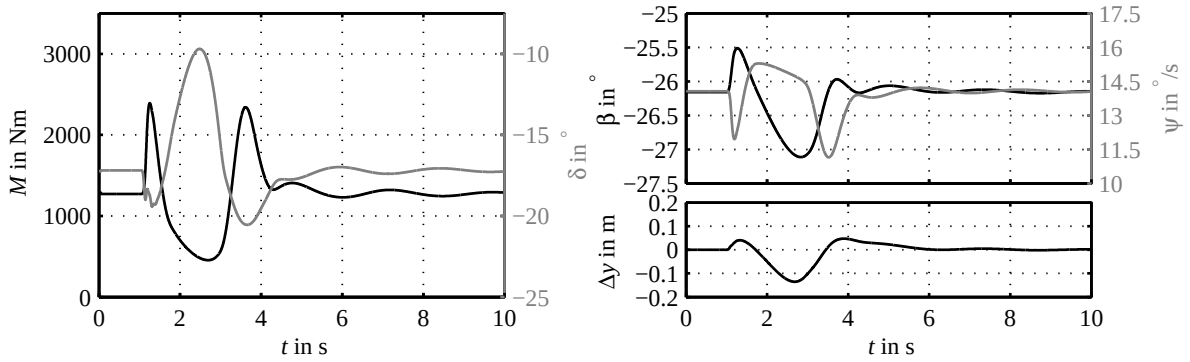

Figure 5 Driver inputs M and δ, vehicle side slip angle β and yaw rate $\dot{\psi}$, predicted future path deviation Δy

Eigenvalue/vector analysis (of the four-wheel vehicle model) of regular driving in point R reveals a stable motion. When the motion is destabilized however, the positive complex pair of eigenvalues and the components of the corresponding eigenvectors show, that above all, yaw rate and vehicle side slip angle oscillations are excited. The powerslide motion in point P is characterized by a monotone instability indicated by two positive, real eigenvalues, $\lambda_1 \ll 1$, λ_2. Modal controllability analysis at point P shows, that the relevant, unstable, monotone mode corresponding to λ_2 is mostly affected by steering input. In point P the corresponding eigenvectors have only small components related to yaw rate and vehicle side slip angle. As a consequence, the powerslide instability may be handled easier by the driver.

It should be mentioned, that due to a control design based on locally linearized system equations, only moderate disturbances can be handled by the driver model. Time delays and limitations from the drive line are not yet considered. Typical steering frequencies of the driver of about 0.3–0.6 Hz for regular driving, may be shifted to about 1 Hz, as indicated by measurements from powerslides with expert drivers, [5].

6 CONCLUSION

While handling characteristics at regular driving conditions are typically influenced by (elasto)kinematics of the suspension systems and the tyre characteristics, the latter is in particular import for the nature of the handling characteristics at extreme driving conditions, like the powerslide. To simulate a powerslide motion of a vehicle with rear-wheel drive, lateral saturation properties of the rear tyres need to be modelled, as well as the related influence of the longitudinal slip due to large traction forces. For realistic behaviour wheel load transfer front/rear, left/right, has to be taken into account. The unstable powerslide motion is stabilized by a human-like driver model, applying appropriate steering and/or throttle inputs. Also the driver's path tracking capabilities have been considered in the presented driver model.

References

[1] H.B Pacejka: *Simplified analysis of steady-state turning behaviour of motor vehicles. Part 1. Handling diagrams of simple systems*, Vehicle System Dynamics **2**, 161–172, 1973.

[2] H.B Pacejka: *Simplified analysis of steady-state turning behaviour of motor vehicles. Part 2. Stability of the steady-state turn*, Vehicle System Dynamics **2**, 173–183, 1973.

[3] M. Abdulrahim: *On the Dynamics of Automobile Drifting*, SAE paper no. 2006-01-1019, 169–178, 2006.

[4] J. Edelmann, M. Plöchl, P. Lugner, W. Mack and A. Falkner: *Investigations on the powerslide of automobiles*, in: Proc. of AVEC 2008, Kobe, 2008.

[5] J. Edelmann and M. Plöchl: *Handling characteristics and stability of the steady-state powerslide motion of an automobile*, Regular and Chaotic Dynamics **14**, 682–692, 2009.

[6] R.Y. Hindiyeh and J.C. Gerdes: *Equilibrium analysis of drifting vehicles for control design*, in: Proc. of ASME 2009, Hollywood, 2009.

[7] C. Voser, R.Y. Hindiyeh, J.C. Gerdes: *Analysis and control of high side slip maneuvers*, Vehicle System Dynamics **48** Supplement 1, 317–336, 2010.

[8] E. Velenis, E. Frazzoli and P. Tsiotras: *Steady-state cornering equilibria and stabilisation for a vehicle during extreme operating conditions*, Int. Journal of Vehicle Autonomous Systems **8**, 217–241, 2010.

[9] E. Velenis, D. Katzourakis, E. Frazzoli, P. Tsiotras and R. Happee: *Stabilisation of Steady-State Drifting for a RWD Vehicle*, in: Proc. of AVEC 2010, Loughborough, 2010.

[10] E. Velenis and P. Tsiotras: *Minimum Time vs Maximum Exit Velocity Path Optimization During Cornering*, in: Proc. of IEEE Int. Symp. on Industrial Electronics, Dubrovnik, Croatia, 2005.

[11] H. Nozaki: *Driver steering model and improvement technique of vehicle movement performance during drift running*, Automotive Technology **7**, 449–457, 2006.

[12] W. Kortüm and P. Lugner: *Systemdynamik und Regelung von Fahrzeugen*, Berlin: Springer, 1994.

[13] S. D. Keen and D. J. Cole: *Application of time-variant predictive control to modelling driver steering skill*, Vehicle System Dynamics **49**, 527–559, 2011.

[14] J. Edelmann, M. Plöchl, W. Reinalter and W. Tieber: *A passenger car driver model for higher lateral accelerations*, Vehicle System Dynamics **45**, 1117–1129, 2007.

[15] D. T. McRuer, D. Graham, E. S. Krendel and W. Reisner: *Human pilot dynamics in compensatory systems: theory, models and experiments with controlled-element and forcing function variations*, Wright-Patterson Air Force Base (OH): Technical Report AFFDL-TR-65-15, 1965.